More than skin deep: sea surface temperature as a means of inferring Atlantic Water variability on the southeast Greenland continental shelf near Helheim Glacier

T. Snow[1,2], F. Straneo[3], J. Holte[3], S. Grigsby[1,4], W. Abdalati[1,2], T. Scambos[1]

[1]Cooperative Institute for Research in Environmental Sciences, University of Colorado, Boulder, CO, USA
[2]University of Colorado Boulder, Geography Department, Boulder, CO, USA
[3]Scripps Institution of Oceanography, University of California San Diego, La Jolla, CA, USA
[4]Department of Geophysics, Colorado School of Mines, Golden, CO, USA

Key Points:

- Sea surface temperatures measure upper ocean temperatures after variability tied to the atmosphere is removed
- Once adjusted for air temperature, Shelf Trough sea surface temperatures infer deep Atlantic Water temperatures near Sermilik Fjord
- Dilution of Atlantic Water as it intrudes onto the continental shelf modulates nearshore temperatures

Corresponding author: Tasha Snow, tasha.snow@colorado.edu

Abstract

Outlet glaciers account for almost half of the Greenland Ice Sheet's mass loss since 1990. Warming subsurface Atlantic Water (AW) has been implicated in much of that loss, particularly along Greenland's southeastern coast. However, oceanographic observations are sparse prior to the last decade, making it difficult to diagnose changes in AW properties reaching the glaciers. Here, we investigate the use of sea surface temperatures (SST) to quantify ocean temperature variability on the continental shelf near Sermilik Fjord and Helheim Glacier. We find that after removing the short-term, atmospheric-driven variability in non-winter months, regional SSTs provide a reliable upper ocean temperature record. In the trough region near Sermilik Fjord, the adjusted SSTs correlate well with moored ocean measurements of the water entering the fjord at depth and driving glacier melting. Using this relationship, we reconstruct the AW variability on the shelf dating back to 2000, eight years before the first mooring deployments. Seasonally, AW reaches close to the fjord's mouth in fall and winter and further offshore in spring. Interannually, the AW temperatures in the trough do not always track properties in the source waters of the Irminger Current. Instead, the properties of the waters found at the fjord mouth depend on both variations in the source AW and, also, in the Polar Water that flows into the region from the Arctic Ocean. Satellite-derived SSTs, although dependent on local oceanography, have the potential to improve understanding around previously unanswered glacier-ocean questions in areas surrounding Greenland and Antarctica.

Plain Language Summary

Greenland ice contributes one-quarter of global sea level rise each year and almost half of that loss comes from glaciers at its periphery. Warming ocean waters may cause much of that loss. Measurements made by ocean instruments serve as the predominant method for studying the oceans around Greenland, but few observations exist prior to the last decade. In this work, we investigate the use of sea surface temperatures acquired by satellites to assess ocean temperature changes through time. We explore their use near the southeastern Greenland coast, where warm water circulates from the North Atlantic Ocean onto the continental shelf and eventually reaches Helheim Glacier, Greenland's fifth largest glacier. Through a comparison with ocean instruments, we find that sea surface temperatures serve as a good indicator of upper ocean temperatures in this region

once proper corrections are applied. With these records, we find that the dilution of warm waters as they circulate from the North Atlantic changes over time and governs the temperature of the water that eventually reaches Helheim, which was previously unknown. Our work shows that sea surface temperatures can provide new insight into the ocean changes that may have impacted glacier retreat before ocean instruments were deployed.

1 Introduction

The Greenland Ice Sheet and its surrounding oceans have changed rapidly as a result of shifting climate conditions in recent decades (Shepherd et al., 2012; The IMBIE Team, 2019). Since the late 1990's, many of Greenland's tidewater glaciers have experienced periods of substantial thinning and retreat, interspersed with periods of greater stability and partial re-advance (Howat et al., 2008; Moon et al., 2012). Almost half of the ice sheet mass loss occurs at marine-terminating outlet glaciers (Rignot & Kanagaratnam, 2006; van den Broeke et al., 2009; Enderlin et al., 2014; The IMBIE Team, 2019) and changes in total ice sheet discharge appear to be related to shifts in outlet glacier frontal position (King et al., 2018). Enhanced submarine melting driven by ocean warming has been implicated in many recent glacier front retreat events (Walsh et al., 2012; Straneo & Heimbach, 2013; Millan et al., 2018), such as at Jakobshavn Isbræ (Holland et al., 2008), Zachariae Isstrom (Mouginot et al., 2015), Kangerdlugssuaq (Christoffersen et al., 2011; Inall et al., 2014; Bevan et al., 2019), and Helheim Glacier (Howat et al., 2008). These glaciers alone accounted for more than 40% of Greenland's excess discharge, as opposed to surface runoff, between 2000 and 2012 (Enderlin et al., 2014). However, the changes in ocean circulation leading to these glacier retreat events is generally weakly characterized. Changes in ocean temperature and volume transport near Greenland's tidewater systems were mostly unmonitored during many earlier events.

Sermilik Fjord abuts Helheim Glacier, one of Greenland's largest glaciers (Enderlin et al., 2014). The region is among the best instrumented and well understood glacier-ocean systems (Straneo et al., 2016), making it an ideal area to investigate the extent to which sea surface temperature variability may be used to infer ocean variability in the vicinity of an outlet glacier, where oceanographic thermal characteristics can be of great significance. Sermilik experiences highly variable ocean circulation and heat transport within the fjord and on the continental shelf (Straneo et al., 2010; Sutherland et al., 2013; Jackson et al., 2014). Heat is primarily delivered by relatively warm, saline Atlantic Wa-

ter (AW; ∼2.0-5.2°C, >150-250 m) from the Irminger Current (IC) offshore of the continental shelf break (Straneo et al., 2010; Jackson et al., 2014). The IC carries AW equatorwards at the surface and extending down to depths greater than 500 m (Rudels et al., 2002; Johannessen et al., 2011; Våge et al., 2011; Andresen et al., 2012). Along the inner shelf, the East Greenland Coastal Current (EGCC) is a low salinity wedge perched atop deeper AW (Bacon et al., 2002; Sutherland & Pickart, 2008). Above 150-250 m, the upper layer carries cold and fresh Polar Water (PW; <4°C) exported out of the Arctic and the northeastern Greenland fjords, including Sermilik (Bacon et al., 2002; Sutherland & Pickart, 2008; Harden et al., 2014). The EGCC flows south, 20-30 km wide, hugging the Greenland coastline (Sutherland & Pickart, 2008). Transport within the EGCC varies seasonally with the greatest freshwater transport in December and generally higher transport in winter and spring coinciding with its speedup and deepening (Sutherland & Pickart, 2008; Bacon et al., 2014; Harden et al., 2014; Le Bras et al., 2018). IC and EGCC variability on the shelf can influence water properties in Sermilik Fjord and, therefore the glacier front; however, the oceanographic studies in the region are mostly recent. Past ocean variability on the shelf and within the fjord is largely unknown before the record that began in 2008 (Straneo et al., 2016), years after thinning and retreat occurred at Helheim Glacier (Howat et al., 2005; Luckman et al., 2006).

While the EGCC and IC have been relatively well studied, the interactions between them in the region outside of Sermilik Fjord, and the temporal variability in those interactions, are poorly understood as a result of limited spatial and temporal measurement coverage. From summer shipboard surveys and longer-term mooring deployments, research in this area has suggested that seasonality in EGCC current width, depth, and transport along the shelf is controlled by alongshore winds (Sutherland & Pickart, 2008; Harden et al., 2014; Le Bras et al., 2018). The PW layer across the shelf thickens through winter and spring (Straneo et al., 2010; Bacon et al., 2014), likely caused by increasing freshwater transport from the Arctic (Harden et al., 2014). Warm AW (2.0-5.2°C, >150-250 m; Jackson et al., 2014) encroaches onto most of the shelf below PW throughout the year, often via troughs that cut across the continental shelf and into the fjords at depth (Rudels et al., 2002; Sutherland et al., 2013). The AW near the coast is cooler than at the shelf break likely as a result of surface cooling and mixing with PW (Straneo et al., 2012). Aside from this general AW inflow at depth, AW can flow onto the shelf as a full-depth layer via occasional AW intrusions within the troughs or seasonally-varying in-

flow across portions of the shelf (Sutherland et al., 2013; Harden et al., 2014). This seasonal inflow intensifies in the fall and is associated with a narrower EGCC banked up against the coast (Harden et al., 2014). Straneo and Heimbach (2013) have posited that more frequent AW intrusions may lead to warmer waters on the inner shelf, and greater influence of AW on the shelf links to increased glacier calving activity (Andresen et al., 2012). All past work in this region is limited spatially or temporally relative to the scale of the overall study region, which extends ∼200 km between the coast and continental shelf break. As a result, little is known about the variability of the AW across much of the shelf and its influence on inner shelf and fjord water temperatures. However, it is clear that AW inflow strongly influences heat transport onto the shelf (Sutherland et al., 2013; Harden et al., 2014) and into the fjord (Straneo et al., 2010; Jackson et al., 2014).

The availability of sea surface temperature (SST) records from the period prior to the speed up of many Greenland glaciers that occurred in the early 2000s raises the possibility of inferring oceanic variability at Greenland's glacial margins through proxies that are built on SSTs. Several recent studies have attempted to define this relation largely through correlations of glacier activity and SST variability with mixed results. Warm SSTs and sea ice variability have been correlated with glacier front changes (Howat et al., 2008, 2010; Johannessen et al., 2011; Andresen et al., 2012; Schild & Hamilton, 2013; Khan et al., 2014), but important questions remain about the extent to which SSTs around Greenland provide information about the subsurface water column where the AW, which influences submarine melting of the larger glaciers, resides. Important progress on that front has been made by Sutherland et al. (2013) who found that, for the period from 2004-2010, summertime (JJA) MODerate resolution Imaging Spectroradiometer (MODIS) SSTs on the continental shelf near Sermilik Fjord correlated closely with tagged-seal temperature measurements at 50 m depth, with diminishing correlation at deeper depths until decoupling below 250 m. However, a broader treatment is necessary in order to constrain temporal variations in ocean temperatures, which is crucial for discerning ice-ocean interactions in glacier retreat events back through time. SSTs have been hitherto underutilized in glacier change analysis and may provide observations that complement temporal and spatial gaps of *in situ* measurements.

Here, we investigate the use of SSTs as a means of assessing the variability of the subsurface waters that enter Greenland's glacial fjords and melt glaciers at depth (Straneo et al., 2012). Differently from other studies we make use of oceanographic subsurface data

to investigate the correlation between surface properties in different regions on the shelf, in the vicinity of Sermilik Fjord, and those observed at depth at the mouth of the fjord. We derive a proxy for subsurface AW temperatures using SSTs adjusted for local air temperatures to produce the first AW record near Sermilik dating back to 2000. We also track AW intrusion variability along the trough leading to Sermilik Fjord to give insight into the drivers of subsurface AW temperature changes on the shelf. While our findings are specific to the oceanography of this region, our analysis demonstrates that SSTs provide novel insight into ocean variability and hold promise for addressing long-standing glacier-ocean questions around both ice sheets.

2 Data and Methods

2.1 Satellite-Derived Sea Surface Temperatures

In contrast to the spatially and temporally limited *in situ* data, SSTs acquired from satellites offer an untapped and potentially illuminating resource for tracking ocean temperature and extent of AW inflow onto the continental shelf. To help reconstruct ocean variability here, we use MODIS-derived SSTs, which provide the temperatures of the ocean skin (upper few μm; SST_{skin}; see Figure S1). The accessibility of MODIS SST products, the instrument's moderate spatial resolution, and its ∼15 scans per day by each of the two satellites on which it flies (Aqua and Terra) provides extensive spatiotemporal coverage suitable for our objectives. In this work we use the MODIS Aqua and Terra Daily Global Level 3 4-km Mapped Thermal daytime and nighttime SST R2014.0 products (quality level 0 and 1) derived from the 11 and 12 μm thermal infrared (IR) channels 31 and 32, respectively (Kilpatrick et al., 2015; Ocean Biology Processing Group, 2014a, 2014b). The data we use span the period beginning Feb 24, 2000 for Terra and July 4, 2002 for Aqua, and ending Dec 31, 2018 for both satellites. The retrieval error for the SSTs is ∼0.4°C (Kilpatrick et al., 2015). We reference the four MODIS SST products hereafter based on their division by satellite and time of day: Terra daytime (T-D), Terra nighttime (T-N), Aqua day (A-D), and Aqua night (A-N).

Before extracting SSTs from each of the four products, we account for cloud and sea ice contamination that may occur because the MODIS SST processing pipelines are not optimized for polar climates (Kilpatrick et al., 2019; Jia, 2019, see Supplementary Information). Arctic SSTs can have cloud contamination (Kilpatrick et al., 2019) that

can introduce noise by shifting SST retrievals toward an artificially cold measurement (Ackerman et al., 1998). To reduce these effects, we apply a mask for clouds and ensure further robustness by applying spatial and temporal averaging for each sampling region and across multiple SST products, as described below. Sea ice contamination can also lead to a cool bias in the SST retrievals, and we find that the daytime SST products, especially in Aqua, contain systematically more sea ice contamination (Figure S2a). To reduce sea ice misclassification and these inter-product differences, we apply a separate sea ice mask, created from MODIS and passive microwave sea ice products, to the four daily SST products (see Supplementary Information).

2.2 Sampling Regions

To investigate SST spatial and temporal variability near Sermilik Fjord, we examine three regions: the IC, EGCC, and the Shelf Trough (ShTr) region (Figure 1). We chose the IC and EGCC sampling regions based on the observations from Rudels et al. (2002) and Sutherland and Pickart (2008) that characterize the locations of the currents, respectively, and chose the boxes' sizes to include relatively homogenous SSTs based on the SST climatology from the region. We use IC and EGCC regions as indicative of AW and PW end members, respectively, because these are the primary water masses at the surface in the respective boxes (Rudels et al., 2002; Sutherland et al., 2013). In addition, we define a 'ShTr region' over the trough leading to Sermilik Fjord, where AW flows onto the shelf and mixes with the EGCC (Sutherland et al., 2013). Results for the three regions are not sensitive to small changes in the box locations and size.

2.3 Seasonal and Diurnal Biases

Seasonal differences in instrument scan coverage between the Level 3 MODIS SST products must be accounted for before they can be used to investigate ocean variability in polar regions. Each MODIS instrument acquires 12-18 scans of our study region each day. During the summer solstice, few are classified as nighttime and most scans are binned into the daytime product (Figure S2b). The opposite is true during the winter solstice. As there is a far higher likelihood of getting at least one sea ice- and cloud-free measurement during a day with more scans, this disparity in scan coverage between seasons means the day products (daily, 8-day, monthly, annual) are skewed to summer measurements and night toward winter. As a result of these differences, creating a robust

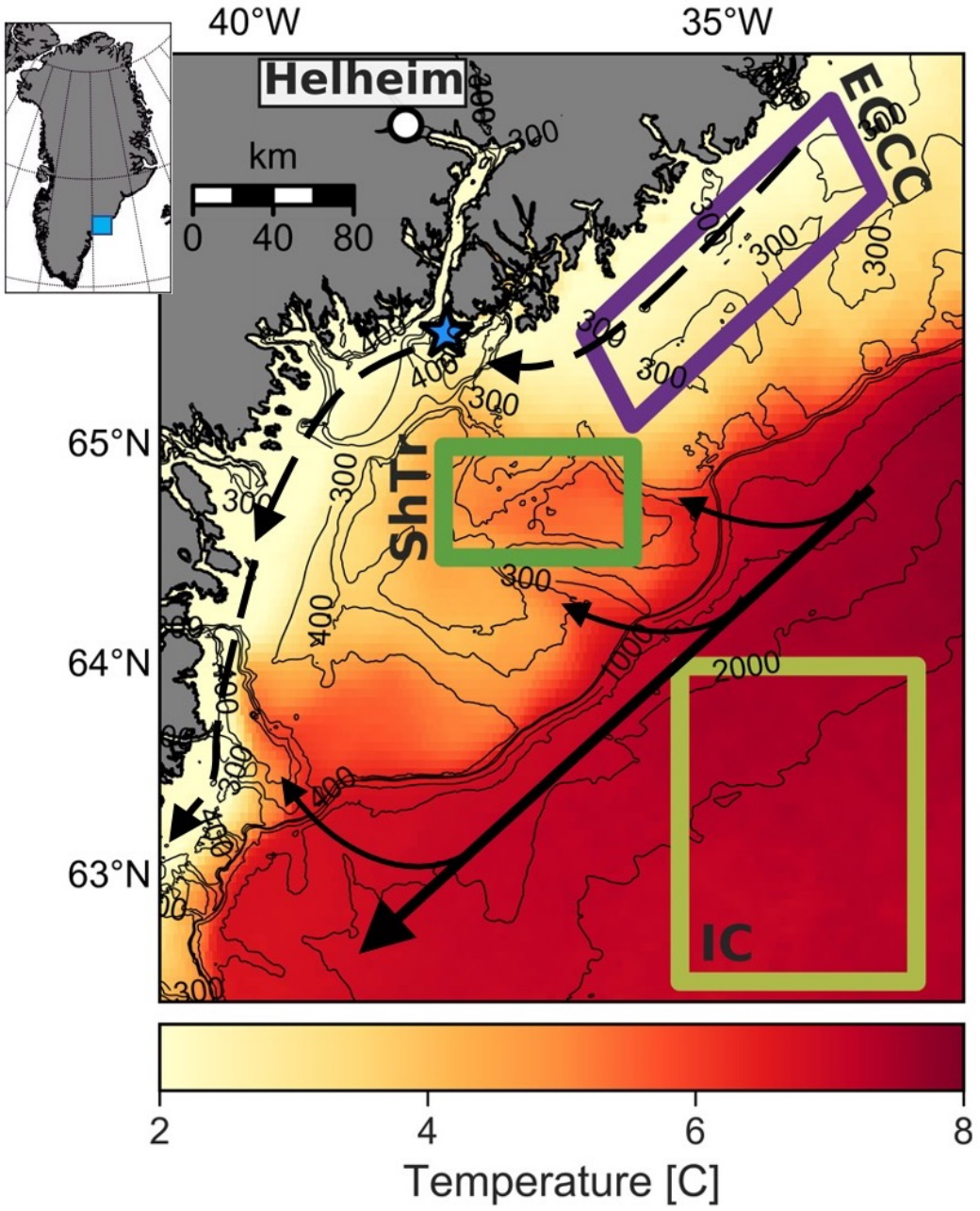

Figure 1. 2000-2016 mean nighttime MODIS SST of the Ammassalik region around Sermilik fjord. Solid black arrows show the location of the Irminger Current (IC) and dashed show the East Greenland Coastal Current (EGCC), which mix across the Shelf Trough (ShTr) region. Boxes indicate areas over which SST is averaged for each region, the blue star shows the trough mooring, and the white circle marks Helheim Glacier. Bathymetry from BedMachine v3 is in thin black lines at 300, 400, 500 m, and every 500 m thereafter (Morlighem et al., 2017).

and continuous record of SSTs that is representative of all seasons requires creating a composite by combining day- and nighttime SSTs for each region.

The day and night products carry inherent biases based on diurnal differences in the SST_{skin}, which we remove before combining the datasets into a composite. Diurnal biases cause a decoupling between the ocean skin and underlying water (Price et al., 1986; Donlon et al., 2002; Minnett, 2003). They are expected as a result of differences in diurnal thermocline and skin temperature effects on the SST_{skin} between day- and nighttime, which also vary seasonally (e.g. Sverdrup et al., 1942; Koizumi, 1956; Eastwood et al., 2011). We calculate the diurnal bias based on differences between the day and night products for each region separately. To determine the biases, we first take the mean of the pixels in the sampling boxes and produce daily time series from 2000-2018 for each of the four masked daily products (Figure 1). We average the A-D and T-D products together to produce a daytime average for each region. We do the same for the two nighttime products. From these records, we produce a day- and nighttime climatology for each of the sampling regions using monthly means across the entire 19-year record (Figure 2). We calculate standard error for the climatologies between the 19 years of monthly data. We define the seasonally-varying diurnal bias as the systematic warm bias in the day products in comparison to the night records across the climatologies (0.28°, 0.39°, 0.46°C for the IC, ShTr, and available EGCC time period, respectively; see Supplementary Information). We use the seasonally-varying diurnal biases for each sampling location – which result from wind speed and solar radiative forcing (Kawai & Wada, 2007) – and subtract them from the day product.

With the diurnal bias removed from the daytime records so that they are equivalent to the nighttime, we assume that all four records represent the bulk SST temperature (Figure S1; Sutherland et al., 2013) and can be combined into a composite record. This assumption for nighttime SST_{skin} is consistent with Minnett (2003) and used by others (e.g. Kilpatrick et al., 2015; Jia, 2019). We hereafter refer to this bulk temperature as the *SST*, although the measurement should also still contain a slight and constant cool skin bias to bulk temperatures as a result of heat flux to the atmosphere (∼0.17°C; Donlon et al., 2002). We average the nighttime and corrected daytime records to produce the composite daily *SST* time series for each region (Figure 2b). From these, we produce weekly and monthly mean SST time series that we use for the rest of our analyses.

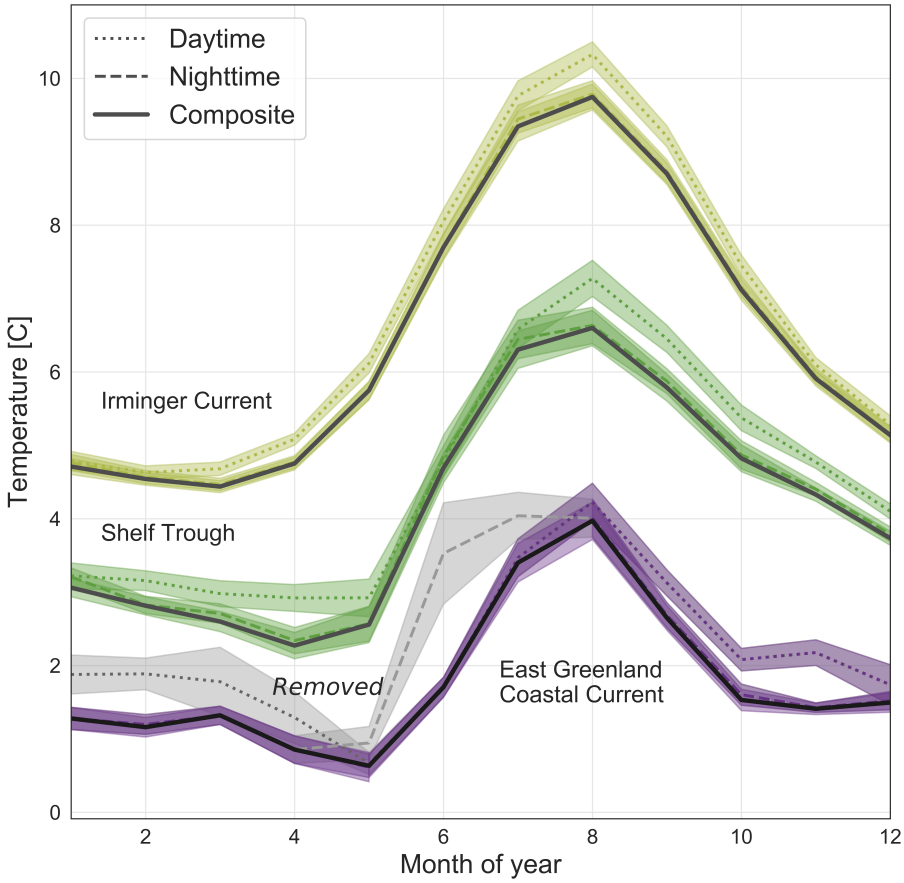

Figure 2. Monthly sea surface temperature climatologies for the 2000-2018 period for the three regions. The IC (yellow), ShTr (green), and EGCC (purple) records are shown for the averaged daytime products (dotted) and nighttime products (dashed). Solid lines show the climatology of the composite after the diurnal bias has been subtracted from the daytime record. Standard error for the nineteen years is shown as shading for each.

2.4 Air and Ocean Temperature Records

To determine the extent to which variability in satellite-derived SST can be used to reconstruct upper ocean temperature outside Sermilik Fjord, we consider two factors that influence SST variability. The SST depends heavily on the depth, magnitude, and history of thermal gradients and stratification at the surface (Donlon et al., 2002, see Figure S1). These properties are controlled by solar heating, heat exchange with the atmosphere, and heat exchange with deeper waters (e.g. Donlon et al., 2002; Minnett, 2003).

SST will therefore be impacted by and potentially covary with both atmospheric and ocean mixed layer temperature changes (e.g. Frankignoul & Hasselmann, 1977; Jaswal et al., 2012).

We use European Center Medium-Range Weather Forecasts (ECMWF) ERA-5 operational reanalysis dataset (Hersbach et al., 2020; Copernicus Climate Change Service, 2017) to assess the relationships between *SST* and air temperatures in each region. From ERA-5, we use the 2-m air temperature measured at 6-hourly time-steps on a 0.5°x 0.5°grid. Air temperatures vary significantly across our study region and are, thus, averaged for each of the *SST* sampling areas, separately.

To determine subsurface water temperature variability on the inner-shelf below the EGCC, we use data from a mooring deployed multiple times between August 24, 2009 - August 18, 2013 on the continental shelf within the trough that leads to Sermilik Fjord (Jackson et al., 2014; Harden et al., 2014; Jackson & Straneo, 2016). From the mooring, we use the temperatures recorded by one instrument each year, either a Microcat SBE37SM or XR 420 RBR sensor, deployed between 264 and 305 m. These temperatures provide a time varying record of subsurface AW that is known to flow into Sermilik Fjord (Straneo et al., 2011; Jackson & Straneo, 2016).

3 Results

3.1 Seasonal and Interannual

The seasonal *SST* records for the three sampling regions are similar but have offsets and different amplitude ranges (Figure 2). Across the 19-year record, the IC is warmest on average (6.5°C) and the EGCC coolest (2.3°C), with ShTr temperatures between them (4.3°C). Similarly, the IC has the largest seasonal range (5.3°C), with the ShTr and EGCC having progressively smaller ranges (4.3°C and 3.3°C, respectively). Across the entire record, the seasonal cycle dominates the interannual variability for the three regions, especially for the IC and ShTr (Figure 3). The interannual variability of the EGCC is slightly more prominent because the EGCC has a smaller seasonal signal.

Seasonally, all three regions experience peak temperatures in August, while the timing of the minimum occurs at slightly different times (Figure 2). The IC experiences a March *SST* minimum and a more sinusoidal seasonal cycle consistent with seasonal ra-

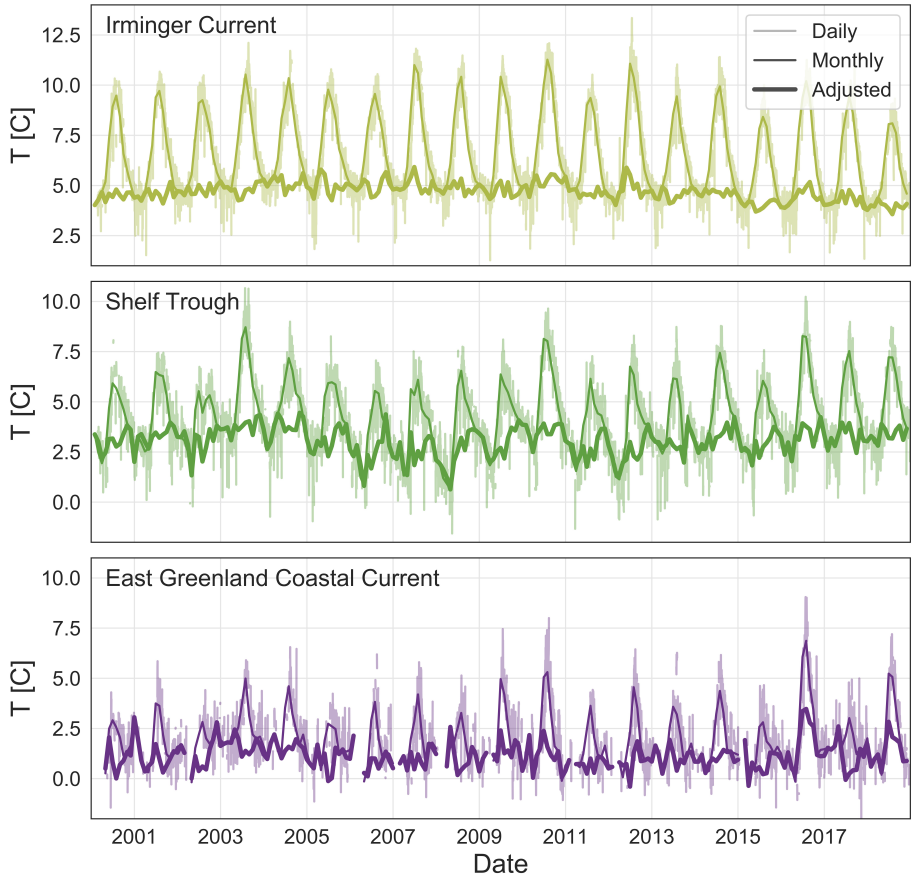

Figure 3. Composite and adjusted *SST* records for each sampling area. Monthly mean (medium) and daily (thin) *SST* composite records for the IC (yellow), ShTr (green), and EGCC (purple) boxes are shown. The *SST* adjusted for air temperature is shown as thick lines (see text for description).

diative forcing. The ShTr and EGCC have a slight cooling trend in winter and spring with a steep transition into warming after reaching minimum temperatures in April/May (ShTr) and May (EGCC). The EGCC minimum lags the ShTr by ∼20 days. The late transition from winter cooling into warming near the coast is consistent with the influence of sea ice (Hastings, 1960), freshwater runoff (Sutherland et al., 2009), and other water-stratifying processes inshore (e.g., weaker winds; Oltmanns et al., 2014; Moore et al., 2015).

3.2 Dependence on Air Temperature

To determine the controls on *SST* variability near Sermilik Fjord, we compare the *SST* with ERA-5 air temperature records (Figure 4, S3). We use ordinary least squares (OLS) regression to examine the linear relationships between air temperature and *SST* in each of the regions separately (Seabold & Perktold, 2010). Through continuous heat exchange, surface air temperature and upper ocean co-variability can have time scales of hours (e.g., diurnal solar heating and turbulence) to a few days (e.g., inertial mixed layer currents; Garwood, 1979; Donlon et al., 2002). We use weekly averages, rather than daily, in the regression to account for both timescales.

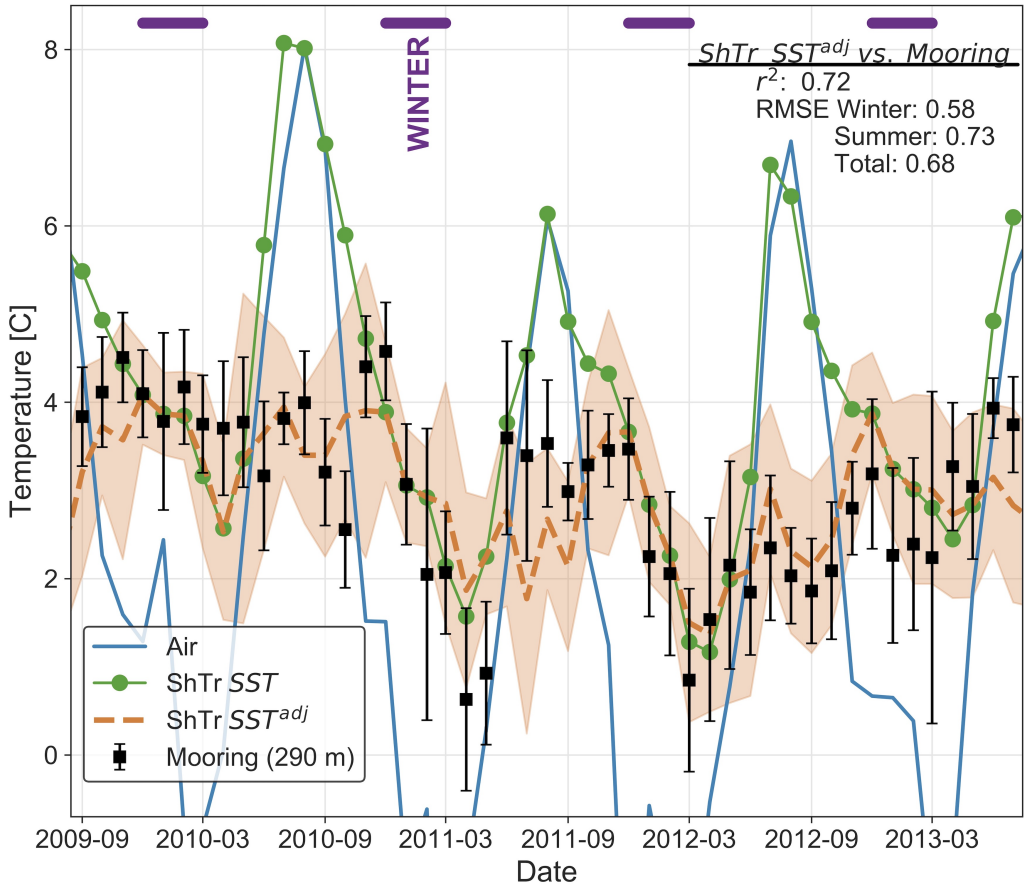

Figure 4. The 'fjord mouth' subsurface water temperature proxy (ShTr SST^{adj}) compared to heat sources. Monthly Shelf Trough *SST* (green) and *SST* adjusted for air temperature (SST^{adj}; orange) - which we identify as a fjord mouth subsurface proxy - are compared to mooring water temperatures from 290 m (black) and air temperatures (blue). The root mean square error (RMSE) between SST^{adj} and mooring temperatures are given. Standard deviations for the ShTr SST^{adj} and mooring temperatures are shown as orange shading and error bars, respectively. Winter (purple) months are shown. Not shown, air temperature reaches -1° to -6°C each winter.

Using an OLS regression model, we find that weekly *SST* in all regions are strongly correlated to ERA-5 air temperature records in summer, but that this relationship does not hold in winter (Figure 4, S3). For example, ShTr *SST* has a strong linear relationship (r^2=0.48) with weekly air temperatures in summer (JJAS; slope=0.71±0.04; Figure S3b), but the relationship becomes weak or insignificant (r^2=0.03) during winter months (DJFM; slope=0.07±0.02). For the remaining months (Apr, May, Oct, Nov), *SST* shows a weaker correlation with air temperature (slope=0.40±0.04; r^2=0.23). Our findings are consistent with a shallower ML or strongly stratified surface ocean in non-winter months, which results in a more closely coupled air-sea temperature response than in winter (Chang, 1993). It is also consistent with previous work that found a weaker coupling between *SST* and air temperature in winter than in summer around Greenland (Singh et al., 2005, 2006). This general relationship holds for all three sampling regions (Figure S3), but the magnitudes and significance of the relationships in some months differ slightly (Table 1). This is expected based on stratification and heating differences between the regions (e.g. Sutherland & Pickart, 2008), which affect ocean skin temperatures and air-sea interactions (Garwood, 1979).

3.3 *SST* on the Shelf and Mooring

We also investigate the connection between ShTr *SST* and the subsurface mooring temperature using the OLS regression model. The ShTr box is a region where AW inflow can extend all the way to the surface (Sutherland et al., 2013). In the regression, we use monthly averages as the most appropriate timescale for comparisons between *SST* and mooring temperatures to account for potential sub-monthly lag times. We find that ShTr *SST* correlates strongly with subsurface water temperatures in wintertime only (Figure 4). Specifically, monthly trough mooring temperatures (290 m) have a significant linear relationship with ShTr *SST* in winter (slope=1.18±0.16, r^2=0.79), but not in summer months (slope=0.23±0.09, r^2=0.18) (Figure S4a). Markedly, the strong relationship between ShTr *SST* and subsurface waters occurs in the months when *SST* shows little linkage to air temperature and the region receives little solar insolation.

We attribute this relationship to the fact that the upper ocean water masses in the ShTr box are linked with those found subsurface at the mooring location further downstream. This is consistent with the results of Sutherland et al. (2013), who showed that full depth AW intrusions occur in the ShTr region and that AW are found subsurface

at the mooring. Conversely, surface waters at the mooring location are indicative of PW properties, consistent with the stratification described by Harden et al. (2014). Based on observed velocities of 0.1-0.6 ms^{-1} (Harden et al., 2014) and wind-driven velocity shifts on synoptic timescales (Jackson et al., 2014), we expect a temperature lag for water transport between the middle of the ShTr box and the mooring site (∼80 km) that may range from a day to more than a week – supporting our choice of focusing on monthly variability. The stronger wintertime mooring/SST relationship is consistent with deepening of the IC wintertime mixed layer as a result of air-sea forcing (Våge et al., 2011; de Jong et al., 2018).

3.4 Upper Ocean Temperatures and a Fjord Mouth Subsurface Water Temperature Proxy

Since SST is significantly correlated with air temperature in non-winter months, consistent with a stronger near-surface stratification, we removed the portion of SST variability related to air temperature to obtain a better indicator of upper layer ocean temperatures. To do this, we build a multivariate linear model that expresses daily (t) SST for each region as the combination of a portion that covaries with air (T^{air}) and one that covaries with upper ocean (T^{ocean}) temperatures:

$$SST_R(t) = A_R^m T_R^{air}(t) + B_R T_R^{ocean}(t) + C_R \tag{1}$$

where A^m is the proportionality coefficient for the relationship between SST and air temperature that varies by month (indicated by the superscript m), B is a constant proportionality coefficient with upper ocean temperatures, and C is a skin bias (expected to be similar to the ∼-0.17 global average; Donlon et al., 2002). We assume that this relationship holds for each of the regions with coefficients that are region dependent and indicated by the subscript R. Physically, $\mathrm{A}^m\mathrm{T}^{air}$(t) represents the variability resulting from air-sea interactions that is a function of the heat exchange between the near-surface ocean layers (dependent on layer thickness), the short and longer term flux of latent and sensible heat through the air-sea interface (dependent on air temperature, ocean temperature, wind speed, and humidity), short- and long-wave radiation through the ocean surface, salinity effects, and horizontal advection (Kraus & Turner, 1967; Denman, 1973; Frankignoul & Hasselmann, 1977). Previous climate modeling work has estimated the linkage between air temperature and SST, sometimes using a simple bias correction (Schulz

et al., 1997) or through more complex relationships that include humidity, and wind speed (Konda et al., 1996; Gautier et al., 1998; Jones et al., 1999; Singh et al., 2006). The relationship between air temperatures and SST is complex, but as we show in Section 4.2 and below, it can be approximated in our study regions as a simple statistical linear relationship. For each region (R), we further define an adjusted SST (SST^{adj}):

$$SST_R^{adj}(t) = SST_R(t) - A_R^m T_R^{air}(t) \tag{2}$$

where $\mathrm{A}^m\mathrm{T}^{air}(\mathrm{t})$ is subtracted to remove the SST variability tied to the atmosphere. We calculate A^m for each region, and each month, using an OLS regression model with a monthly interaction term that finds the slope relationships between monthly SST and air temperatures (Table 1). For months with statistically insignificant slope relationships ($\mathrm{p} \leq 0.05$), we apply A=0; therefore, SST^{adj} is equivalent to SST for some winter months (DJF).

Table 1. A^m parameters parameters calculated by the Ordinary Least Squares Regression models for the ShTr, IC, and EGCC. Number of measurements (N) and R^2 provided for all months of each model. Intercept and insignificant parameters not used for corrections.

Month	ShTr N=965 R^2=0.71	IC N=980 R^2=0.91	EGCC N=776 R^2=0.60
Jan	0.02±0.04	0.02±0.03	**-0.09±0.04**
Feb	0.03±0.04	-0.01±0.03	-0.07±0.05
Mar	**0.12±0.03**	-0.05±0.03	-0.07±0.05
Apr	**0.21±0.06**	0.01±0.02	-0.13±0.09
May	0.02±0.07	**0.21±0.02**	**-0.19±0.08**
Jun	**0.45±0.04**	**0.41±0.01**	**0.12±0.03**
Jul	**0.63±0.02**	**0.53±0.01**	**0.40±0.02**
Aug	**0.58±0.02**	**0.54±0.01**	**0.47±0.02**
Sep	**0.52±0.02**	**0.50±0.01**	**0.36±0.02**
Oct	**0.55±0.03**	**0.44±0.01**	**0.24±0.04**
Nov	**0.57±0.06**	**0.31±0.02**	-0.10±0.06
Dec	0.06±0.05	**0.15±0.02**	**-0.15±0.04**

[a]Bold indicates significant parameters ($\mathrm{p} \leq 0.05$).

The SST^{adj} for the three regions have a wide range of seasonal and interannual variability that we interpret as representing the upper ocean temperature variability (Figure S1). The EGCC and IC monthly and interannual variability (Figure 5) is consistent with ranges in the upper ocean mooring temperatures described by Harden et al. (2014) and de Jong et al. (2018), respectively. Unlike for the absolute SST, the EGCC and ShTr

373 SST^{adj} exhibit a larger variance (0.51°and 0.45°C, respectively) than the IC (0.20°C).
374 This is consistent with synoptic and seasonal upper ocean temperature swings associ-
375 ated with seasonal heating cycles, cold meltwater influx, and variable AW inflow inshore
376 (Straneo et al., 2010; Harden et al., 2014). SST^{adj} temperature ranges are smaller than
377 those of the absolute SST (Figure 3), which is consistent with differences between up-
378 per ocean temperatures and bulk SST (see Figure S1; Chang, 1993).

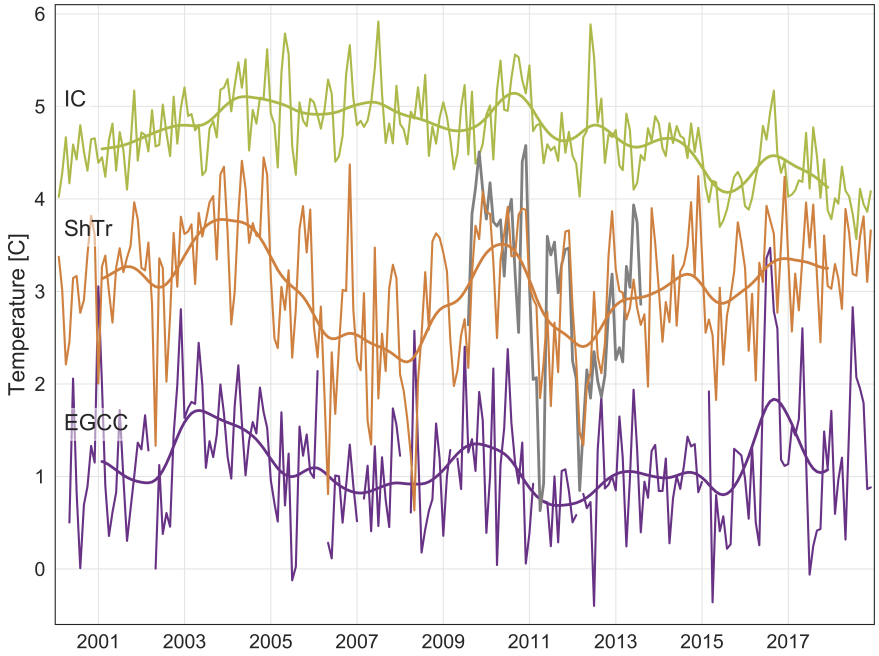

Figure 5. Monthly SST^{adj} records for 2000-2018 for the Irminger Current (yellow), Shelf Trough (orange), and East Greenland Coastal Current (purple). Thin lines are monthly SST while thick lines represent 24 month low-pass Butterworth filtered records for each. The trough mooring temperatures (gray) are shown for comparison. The ShTr SST^{adj} record is a proxy for the trough mooring temperatures.

379 Using a second-order low-pass digital Butterworth Filter (Virtanen et al., 2019),
380 with a 24-month cutoff frequency, we further examine the longer-term SST^{adj} variabil-
381 ity for the three different regions. While we find that the upper ocean layer was warmest
382 in the early 2000's in all three regions, their variability differed in subsequent years. Specif-
383 ically, the IC remained warm from 2005 to 2008, while the ShTr and EGCC experienced
384 a general cooling that was more pronounced for the ShTr than the EGCC. Furthermore,

the ShTr box also continuously warmed after 2012, whereas the IC exhibited long-term cooling, consistent with the deepening of convection in the Irminger Sea and generalized cooling of the subpolar gyre during this period (de Jong & Steur, 2016; de Jong et al., 2018). In general, warmer years in the ShTr record were consistent with IC temperatures, while they more closely resembled EGCC temperatures in the coldest years. Although the upper ocean temperature records for the three regions differed substantially, ShTr SST^{adj} correlated more with the EGCC (r^2=0.31, p<0.001) than the IC (r^2=0.10, p=0.13).

Given that the water column in the ShTr region can be relatively homogenous from surface to depth as a result of full-depth AW layers flowing onto the shelf along the trough (Sutherland et al., 2013; Harden et al., 2014), we investigate the extent to which ShTr SST^{adj} can be used as a proxy for the subsurface water temperatures at depth at the mooring location near Sermilik Fjord mouth, year-round (see Figure 1 for mooring location). We find that the ocean mooring temperatures show a linear relationship with ShTr SST^{adj} (slope=0.98±0.14, r^2=0.51; Figure S4b) that is similar to the wintertime relationship (slope=1.18±0.16) found using the full SST. Non-winter ShTr SST^{adj} resembles the uncorrected wintertime measurements in comparison to mooring temperatures (Figure 4; slope=0.93±0.18, r^2=0.46). We find a strong correlation (r^2=0.69) between ShTr SST^{adj} and mooring temperatures that is also stronger for wintertime measurements (winter RMSE=0.58°C, summer RMSE=0.70°C, total RMSE=0.67°C).

In addition to the correspondence between the mooring data and the adjusted SST in the ShTr region, the fact that the ShTr SST^{adj} is warmest in November and December and coolest from March to May (Figure 6b) is consistent with subsurface temperatures observed on the shelf between 2004 and 2010 using tagged-seals (Straneo et al., 2010). We also find good agreement between ShTr SST^{adj} measurements and shipboard hydrographic surveys within the trough taken each August from 2009-2013 (Harden et al., 2014). Thus, we conclude that the ShTr SST^{adj} derived here is a good proxy for the subsurface ocean temperatures at the fjord mouth and hence of the waters that feed Sermilik Fjord at depth and reach the base of Helheim Glacier.

3.5 AW Encroachment onto the Shelf

As shown in Figure 4 and 5, temperature changes in the ShTr region reflect the combined influence of IC and EGCC temperature variability. Here, we investigate changes

in the AW intrusions onto the continental shelf by examining the occurrence of warm temperatures along the trough that supplies AW to the 'ShTr' region and eventually, at depth, to Sermilik Fjord (Figure 6). Specifically, we consider a transect of thirteen 14 x 14 km boxes along the trough crossing the continental shelf and leading to Sermilik Fjord. Within each of the boxes we subtract the daily IC SST^{adj} temperature from the SST^{adj} in the box to create a "trough anomaly" (Figure 6a). The trough anomaly thus indicates how different the box SST^{adj} is from that of the IC. By doing this, we remove any interannual variability in magnitude due to changes in the IC temperature itself as opposed to more or less AW intruding onto the shelf. A less negative anomaly means that trough waters are almost as warm as those offshore (IC region) while a more negative anomaly means that the trough is considerably colder than the IC. Any box covered in sea ice is assumed to be at the freezing temperature of seawater (-1.8°C). To determine thresholds for quantifying when AW temperatures are present at the surface within the trough, we compare anomalies found for all of the pixels within the IC and EGCC boxes, which represent AW and PW end members, respectively. More than 99% of IC pixels have anomalies above -1.5°C, while anomalies within the EGCC tend to be more negative (Figure S5). Using this distinction, we consider a box to have AW at the surface when weekly trough anomalies are greater than -1.5°C (Figure 6b). We determine the seasonal climatology and annual mean for the location of the -1.5°C contour along the transect, removing the weeks where cloud cover obscures part of the transect and makes identification of the -1.5°C contour uncertain. Our results are not sensitive to slight variations in threshold choices.

Temperature anomalies along the trough exhibit substantial variability on synoptic and seasonal timescales (Figure 6). From the climatology, we show that waters with properties similar to those in the IC box extend shoreward (location of box 3) in fall and early winter (OND) but are found offshore (location of box 8) in spring (AM; Figure 6b). We also find a high degree of variability on weekly timescales (Figure 6c). We interpret instances of small amplitude anomalies in the trough temperatures to be associated with AW inflow onto the shelf. Our observations indicate that AW intrudes deeper along the trough in late fall, bringing surface AW closer to the fjord's mouth, while it remains further offshore in spring. This seasonality, in turn, is consistent with the seasonal variability in the ShTr SST^{adj} (Figure 6b) and with the findings of Sutherland et al. (2013). Intrusion of AW further along the trough coincides with warmer seasonal ShTr SST^{adj} tem-

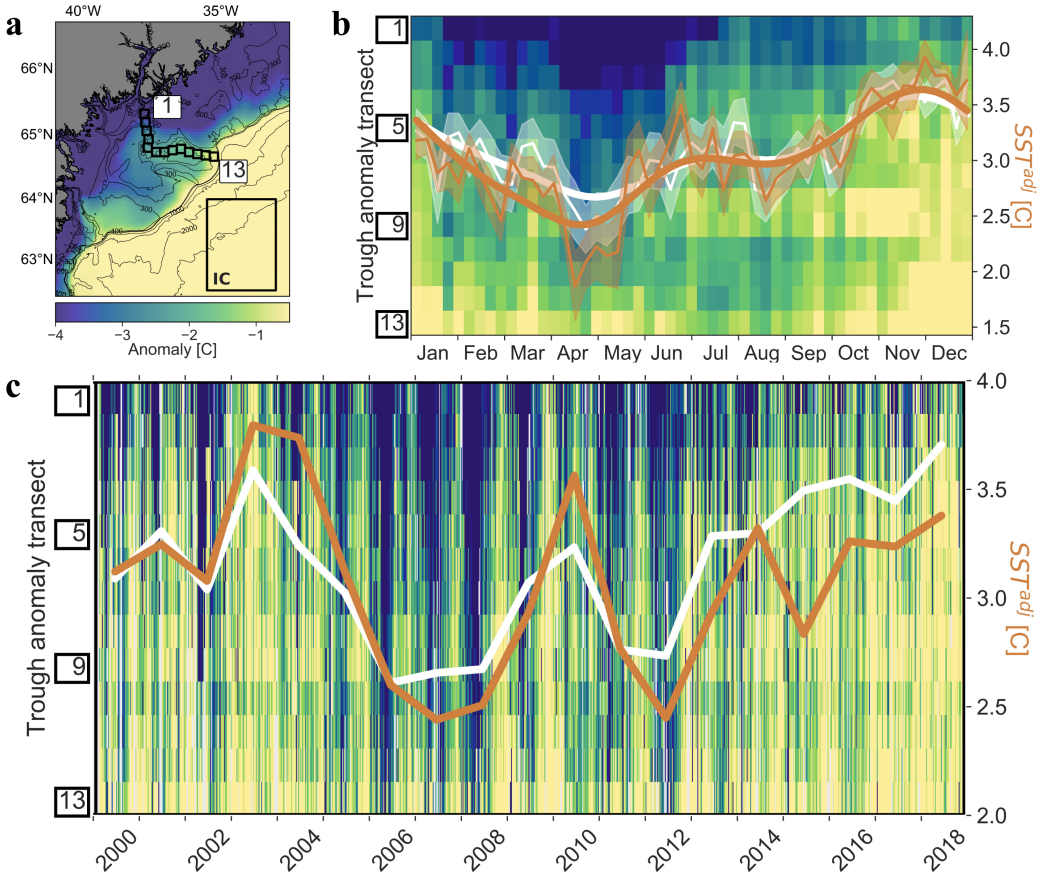

Figure 6. Variability in the trough anomaly along the trough leading to Sermilik Fjord. (a) Map of the 19-year climatological anomaly of SST^{adj} overlain by the thirteen – 14 x 14 km sampling boxes representing a transect from the fjord [1] out to the continental slope [13]. Bathymetry contours from BedMachine v3 (Morlighem et al., 2017). (b) Weekly 2000-2018 climatology of the trough anomaly from (a). The transect from box [1] on the top to [13] at the bottom spans the y-axis and time along the x-axis. The average weekly (thin line) and smoothed (thick line) location of the -1.5°C contour for the trough anomaly (white) is shown in comparison to the same for the ShTr SST^{adj} (orange) with smoothing using a 20-week Butterworth filter. Shading for each shows the standard error for the 19 years. (c) Weekly record for the trough anomaly from 2000-2018. Axes are similar to (b) and the annual means for the -1.5°C trough anomaly location and ShTr SST^{adj} are shown.

peratures (r^2=0.85, p<0.001), although there is a ∼2-week lag between the minimum ShTr SST^{adj} and when AW is furthest offshore.

Interannually, we find that AW spreads furthest inshore in 2003 and 2014-2018, while it is most consistently offshore in 2006-2008 and 2011-2012 (Figure 6c). 2003 and 2018 experienced almost no seasonality, with AW extending along the entire trough (in shore of box 3) nearly year-round. Conversely, PW extended up to the continental shelf-break

for more than half of the year in 2007 and 2008 with little to no AW on the shelf during that time. The extent of AW intrusion strongly correlates with the ShTr SST^{adj} (r^2=0.76, p<0.001), although AW intrudes furthest inshore after 2014, which does not coincide with similarly extreme ShTr temperatures. The earlier periods of stronger intrusion, 2003 and 2010, are consistent with times of anomalously warm IC, however, the later period is not (Figure 4). Explicitly, this means that the variability in heat content of the upper Irminger Sea region (IC box) is not indicative of the extent of AW intrusions onto the shelf. Even as the Irminger Sea has been cooling, in recent years, the AW is intruding deeper onto the shelf and – presumably – influencing the waters flowing into Sermilik Fjord at depth.

4 Discussion

4.1 Reliable Application of Sea Surface Temperatures

While MODIS SSTs provide an under-utilized source of significant insight to oceanic heat transfer to glaciers, significant challenges have slowed widespread application and interpretation of this data trove. Frequent cloud and sea ice cover lead to few measurements of the ocean surface despite the on-average 15 scans acquired per day, and weaknesses in the built-in SST masking protocols mean that the boxed SST products can often have cloud or ice contamination and tendency toward cold biases around Greenland (Szczodrak et al., 2014; Jia, 2019). Regionally, SSTs are influenced by the relatively fresh PW and meltwater found near the coast and in some locations provide little information on the deeper AW temperatures on the continental shelf (Sutherland et al., 2013). Our work, however, shows that with adjustments for diurnal and seasonal variability, SSTs can provide a reliable measure of upper ocean temperatures, and, in the case of Sermilik Fjord, provide a measure of the AW temperatures entering a glacial fjord at depth.

In order to use MODIS skin SSTs in the polar regions as a measure of upper ocean temperatures, additional processing and consideration needs to be given to the Level 3 R2014 SST products provided by the NASA Ocean Biology Processing Group (Jia, 2019). Sea ice must be directly masked (Figure S2a), seasonal skewing by the daytime and nighttime products in polar regions must be accounted for (Figure S1b), and diurnal biases between day- and nighttime products corrected (Figure 2; Minnett, 2003; Kilpatrick et al., 2015). We find that differences between the daytime and nighttime products can be large here and daytime products skew observations towards the summer season when air

temperature changes dominate the SST signal. We also show that SST variability driven by air-sea interactions in non-winter months can be removed to obtain an adjusted SST that is more closely linked with upper ocean temperature (Figure 4). This daytime/summertime bias is important because most previous research using MODIS SSTs around Greenland use daytime products (Howat et al., 2008, 2010; Schild & Hamilton, 2013; Sutherland et al., 2013; Inall et al., 2014), and any research using summertime SSTs (e.g., Murray et al., 2010; Andresen et al., 2012) is likely to be measuring an SST signal strongly tied to atmospheric temperature, rather than the upper ocean.

For the ShTr region only, the resultant SST^{adj} is also found to be representative of temperatures observed at 290 m at a mooring near the mouth of Sermilik Fjord, year-round. We attribute this link to the fact that the AW flowing into the trough are the same which enter the fjord at depth, 80 km downstream, beneath the EGCC, consistent with earlier studies. Our observations are consistent with the findings of Sutherland et al. (2013) who find that 'uncorrected' summertime SST in the ShTr region do not significantly correlate with deeper trough water temperatures – where AW is primarily found – making uncorrected SST unreliable for monitoring them. Once the higher frequency imprinted atmospheric variability in non-winter months has been removed, however, the relationship between these adjusted ShTr SST and subsurface water temperatures becomes significant, albeit with more uncertainty than the respective wintertime relationship (winter RMSE=0.58°C, non-winter RMSE=0.71°C; Figure 4, Figure S4b). For this reason, non-wintertime ShTr SST^{adj} can serve as a useful proxy for tracking subsurface water temperatures flowing into the fjord as long as the higher uncertainty associated with them does not exceed the variability in the ocean temperature signal. This would likely make the non-wintertime subsurface AW estimates inadequate for locations that experience less than a few degrees of water temperature variability.

While ShTr SST^{adj} serve as an estimate for the AW temperatures flowing into the fjord, the connection to deeper waters varies across the region based on differences in stratification, mixing patterns, and water masses present, therefore it is unclear to what extent SST^{adj} can serve as a proxy for subsurface waters in other locations. Many studies have shown large horizontal changes in the properties of the water column between the coast and offshore of the continental break near Sermilik Fjord (e.g., Rudels et al., 2002; Sutherland & Pickart, 2008; Harden et al., 2014). With a strong pycnocline between PW and AW serving as a barrier between the surface and subsurface waters along

the coast (Straneo et al., 2010; Harden et al., 2014), SST^{adj} over the EGCC are indicative of surface PW, and have a much weaker or insignificant connection to the AW flowing below (Table 1). This holds for the EGCC except when intrusions of water from the IC mix horizontally into it, which is not uncommon (Sutherland & Pickart, 2008). Seasonal changes in the stratification and mixing that stem from changes in freshwater input (e.g., sea ice; Stroh et al., 2015), wind speeds, and solar heating (Donlon et al., 2002; Minnett, 2003) will also impact the correlation between SST^{adj} and subsurface waters. Therefore, the choice of SST sampling location heavily impacts what information can be ascertained and the oceanography of each location must be well understood to use SSTs reliably.

4.2 Historical Subsurface Water Temperatures and Implications

Our results provide two key insights about the Sermilik fjord/shelf system. First, AW temperatures offshore within the IC are not necessarily indicative of coastal AW temperatures, which feed Sermilik Fjord. Instead, by the time it reaches the ShTr region, AW is much colder than the IC box, indicating dilution as it crosses the continental shelf (Figure 5). Second, we find that warmer waters intruded further inshore in the early 2000's until early 2005 (consistent with the sediment-based reconstruction of Andresen et al. (2012)), which generally corresponds to changes in discharge patterns at Helheim Glacier (King et al., 2018). These combined observations indicate that the variability in AW temperatures found at depth nearshore result from an interplay of AW intruding onto the shelf and EGCC water - and that the relative fraction of these vary in time. These findings also highlight that satellite-derived SSTs can provide previously unobserved context for spatially or temporally limited field measurements.

Variability observed in the Shelf Trough cannot be explained by IC and EGCC variability taken separately - which represent the AW and PW end members - but is a time-varying combination of the two (Figure 5). Notably, we find that the ShTr SST^{adj} did not always correlate with warmer AW in the IC from which the trough water is derived. The ShTr SST^{adj} instead warms when our analyses show that waters with properties similar to the IC intrude further onto the shelf (Figure 6). This linkage is most notable in the years when the ShTr SST^{adj} cooled while IC temperatures remained warm from 2005-2009 and after 2012 (Figure 6c). We infer that the varying dilution of AW as it crosses the continental shelf controls the ShTr SST^{adj}. These findings suggest that while there

is a direct connection between the North Atlantic Ocean and Sermilik Fjord (Straneo et al., 2010; Andresen et al., 2012), the cooling of AW as it crosses the continental shelf varies interannually, making offshore IC temperatures a poor indicator for the waters entering the fjord.

Within the 19-year record, months with the smallest differences between the ShTr and IC SST^{adj} (Figure 5) are indicative of reduced AW dilution as it crosses the continental shelf (Straneo et al., 2010; Moore et al., 2014). If we take ShTr temperatures to be representative of the AW temperature entering the fjord, this suggests that the waters flowing into the fjord at depth were similar to those in the IC in the early 2000's, briefly in late 2009 to 2010, and in 2014-2018. These were also the years that exhibited the least change in ShTr SST^{adj} across the shelf and, thus, when AW intruded furthest onto the continental shelf (Figure 6c). We hypothesize that years with a more extended intrusion of AW and warmer trough temperatures may also correspond with higher volume transport, but that analysis is outside of the purview of this study.

The ShTr SST^{adj} record indicates that fluctuations in subsurface AW temperature and intrusion coincide with some of the variability in discharge rates previously found at Helheim Glacier for the same time period, but this relationship is not straightforward (Figure 4b). AW spread inshore more consistently and the ShTr SST^{adj} was increasing to their warmest values during the early 2000's when Helheim Glacier experienced ice front retreat (Howat et al., 2005), thinning (Stearns & Hamilton, 2007), and heightened discharge rates (Howat et al., 2007; King et al., 2018). The glacier also decelerated and re-advanced from 2006-2008 (Howat et al., 2007; Schild & Hamilton, 2013) when the ShTr SST^{adj} was the coldest on record, though notably offshore AW temperatures had not measurably changed. In 2010, on the other hand, the ShTr SST^{adj} was relatively warm and AW further intruded, although Helheim did not experience substantial increases in ice discharge (King et al., 2018), which may have been driven by a host of other environmental factors influencing glacier discharge rates (e.g., air temperature, glacier configuration, mélange rigidity; e.g., Joughin et al., 2012; Carr et al., 2013). While more work must be done to investigate mechanisms and the nature of these linkages, our work supports the notion that warmer waters flowing into the fjord from the shelf trough may have played a role in the glacier variability, especially in the early 2000's (e.g., Howat et al., 2008; Millan et al., 2018).

583 The historical context we have constructed using both the ShTr SST^{adj} and trough
584 anomaly record likely have broader applications for understanding the shelf surface and
585 subsurface water temperatures. These waters directly feed the fjord of many deeply grounded
586 outlet glaciers in southeastern Greenland that may share similar AW sources and regional
587 forcings (Straneo et al., 2010; Harden et al., 2014; Jackson et al., 2014; Sutherland et al.,
588 2014; Millan et al., 2018), including three of the largest contributors of ice discharge in
589 Greenland, Helheim Glacier, Kangerdlugssuaq Glacier, and Køge Bugt (Enderlin et al.,
590 2014; King et al., 2018). The applicability of SSTs to specific ice-ocean questions, how-
591 ever, has vast spatial and temporal variability, varies with the SST product used (i.e. day-
592 time or nighttime), and depends heavily on the specific oceanography of the location be-
593 ing explored.

594 5 Conclusions

595 We produce upper ocean temperature records for three regions on the continen-
596 tal shelf near Sermilik Fjord using a composite of the MODIS Level 3 daytime and night-
597 time SST R2014.0 products (Figure 2). We find that SST in the study regions has a monthly-
598 varying linear relationship with air temperature that once adjusted for, produces a record
599 indicative of the upper ocean. The adjusted SST from our Shelf Trough region then have
600 a strong linear relationship with subsurface water temperatures from a mooring located
601 near Sermilik Fjord mouth at 290 m (Harden et al., 2014; Jackson et al., 2014), albeit
602 with higher uncertainty in the summer months (winter RMSE=0.58°C, summer RMSE=0.70°C).
603 This relationship confirms that AW in the Shelf Trough region is linked with subsurface
604 water - which ultimately continues inshore beneath the EGCC to the mooring location
605 where it feeds the fjord. Our records indicate that upper ocean temperatures in all three
606 regions, and at depth in the case of the Shelf Trough, were warmest in the early 2000's
607 when Helheim experienced rapid retreat, supporting previous ideas that ocean warm-
608 ing played a role in the retreat.

609 Comparison of the upper ocean temperature variability in the three regions show
610 that while there is a direct connection between the North Atlantic Ocean and the bathy-
611 metric trough leading to Sermilik Fjord (Straneo et al., 2010), the dilution of AW as it
612 flows across the shelf from the IC varies substantially over long timescales. The extent
613 to which AW intrudes onto the shelf correlates strongly with inferred subsurface AW tem-
614 peratures on the inner-shelf indicating that this intrusion plays a key role in setting the

properties of the heat-carrying waters that flow into Sermilik Fjord at depth. Inferences cannot be directly made between North Atlantic warming and AW changes on the continental shelf near Sermilik Fjord. These findings have important implications for models which seek to resolve ocean temperatures and transport paths within the region.

With proper consideration of the physical processes driving the measurements, SSTs are a relatively untapped tool that show promise in applications to a vast range of polar oceanography and glaciology questions. Further work will continue to expand contextual understanding around the Greenland and Antarctic ice sheets both where long-standing field measurements have been acquired and where none exist.

Acknowledgments

We gratefully acknowledge the National Aeronautics and Space Administration (NASA) and the U.S. National Science Foundation (NSF). This work was supported by NASA Headquarters under the NASA Earth and Space Science Fellowship Program – Grant (NNX16AO33H). This material is also based upon work supported by the NSF Graduate Research Fellowship Program under Grant No. (DGE1650115). Any opinions, findings, and conclusions or recommendations expressed in this material are those of the author(s) and do not necessarily reflect the views of the NSF. Processed data used in this manuscript will be permanently archived at the National Snow and Ice Data Center (nsidc.org). The processing and analysis code is available from the authors on request (tasha.snow@colorado.edu). All mooring data used in this paper is available at the National Oceanographic Data Center (nodc.noaa.gov), Level 3 MODIS SST data can be found at search.earthdata.nasa.gov, and ECMWF ERA-5 data is located at www.ecmwf.int. Thanks also go to the anonymous reviewers for their comments that improved the quality and clarity of this paper.

References

Ackerman, S. A., Strabala, K. I., Menzel, W. P., Frey, R. A., Moeller, C. C., & Gumley, L. E. (1998). Discriminating clear sky from clouds with MODIS. *Journal of Geophysical Research: Atmospheres*, *103*(D24), 32141–32157. doi: 10.1029/1998jd200032

Andresen, C. S., Straneo, F., Ribergaard, M. H., Bjørk, A. A., Andersen, T. J., Kuijpers, A., ... Ahlstrøm, A. P. (2012). Rapid response of Helheim Glacier in Greenland to climate variability over the past century. *Nature Geoscience*,

5(1), 37–41. doi: 10.1038/ngeo1349

Bacon, S., Marshall, A., Holliday, N. P., Aksenov, Y., & Dye, S. R. (2014). Seasonal variability of the East Greenland Coastal Current. *Journal of Geophysical Research: Oceans*, *119*(6), 3967–3987. doi: 10.1002/2013jc009279

Bacon, S., Reverdin, G., Rigor, I. G., & Snaith, H. M. (2002). A freshwater jet on the east Greenland shelf. *Journal of Geophysical Research*, *107*(C7), 5–1-5-16. doi: 10.1029/2001jc000935

Bevan, S. L., Luckman, A. J., Benn, D. I., Cowton, T., & Todd, J. (2019). Warming of SE Greenland shelf waters in 2016 primes large glacier for runaway retreat. *The Cryosphere Discussions*, 1–16. doi: 10.5194/tc-2018-260

Carr, J. R., Stokes, C. R., & Vieli, A. (2013). Recent progress in understanding marine-terminating Arctic outlet glacier response to climatic and oceanic forcing. *Progress in Physical Geography: Earth and Environment*, *37*(4), 436–467. doi: 10.1177/0309133313483163

Chang, P. (1993). Seasonal cycle of sea surface temperature and mixed layer heat budget in the tropical Pacific Ocean. *Geophysical Research Letters*, *20*(19), 2079–2082. doi: 10.1029/93gl02374

Christoffersen, P., Mugford, R. I., Heywood, K. J., Joughin, I., Dowdeswell, J. A., Syvitski, J. P. M., ... Benham, T. J. (2011). Warming of waters in an East Greenland fjord prior to glacier retreat: mechanisms and connection to large-scale atmospheric conditions. *The Cryosphere*, *5*(3), 701–714. doi: 10.5194/tc-5-701-2011

Copernicus Climate Change Service. (2017). *ERA5: Fifth generation of ECMWF atmospheric reanalyses of the global climate.* https://cds.climate.copernicus.eu/cdsapp!/home. (Accessed: 2018-11-04)

de Jong, M. F., Oltmanns, M., Karstensen, J., & Steur, L. d. (2018). Deep Convection in the Irminger Sea Observed with a Dense Mooring Array. *Oceanography*, *31*(1), 50–59. doi: 10.5670/oceanog.2018.109

de Jong, M. F., & Steur, L. d. (2016). Strong winter cooling over the Irminger Sea in winter 2014-2015, exceptional deep convection, and the emergence of anomalously low SST. *Geophysical Research Letters*, *43*(13), 7106–7113. doi: 10.1002/2016gl069596

Denman, K. L. (1973). A Time-Dependent Model of the Upper Ocean. *Journal of*

Physical Oceanography, *3*(2), 173–184. doi: 10.1175/1520-0485(1973)003⟨0173:atdmot⟩2.0.co;2

Donlon, C., Minnett, P., & Gentemann, C. (2002). Toward improved validation of satellite sea surface skin temperature measurements for climate research.

Eastwood, S., Borgne, P. L., Péré, S., & Poulter, D. (2011). Diurnal variability in sea surface temperature in the Arctic. *Remote Sensing of Environment*, *115*(10), 2594–2602. doi: 10.1016/j.rse.2011.05.015

Enderlin, E. M., Howat, I. M., Jeong, S., Noh, M., Angelen, J. H., & Broeke, M. R. (2014). An improved mass budget for the Greenland ice sheet. *Geophysical Research Letters*, *41*(3), 866–872. doi: 10.1002/2013GL059010

Frankignoul, C., & Hasselmann, K. (1977). Stochastic climate models, Part II Application to sea-surface temperature anomalies and thermocline variability. *Tellus*, *29*(4), 289–305. doi: 10.1111/j.2153-3490.1977.tb00740.x

Garwood, R. W. (1979). Air-sea interaction and dynamics of the surface mixed layer. *Reviews of Geophysics and Space Physics*, *7*(17).

Gautier, C., Peterson, P., & Jones, C. (1998). Ocean surface air temperature derived from multiple data sets and artificial neural networks. *Geophysical Research Letters*, *25*(22), 4217–4220. doi: 10.1029/1998gl900086

Gentemann, C. L., Minnett, P. J., Borgne, P. L., & Merchant, C. J. (2008). Multi-satellite measurements of large diurnal warming events. *Geophysical Research Letters*, *35*(22). doi: 10.1029/2008gl035730

Harden, B., Straneo, F., & Sutherland, D. (2014). Moored observations of synoptic and seasonal variability in the East Greenland Coastal Current. *Journal of Geophysical Research: Oceans*, *119*(12), 8838–8857. doi: 10.1002/2014JC010134

Hastings, A. D. J. (1960). ENVIRONMENT OF SOUTHEAST GREENLAND. doi: 10.21236/ad0251797

Hersbach, H., Bell, B., Berrisford, P., Hirahara, S., Horányi, A., Muñoz-Sabater, J., ... Thépaut, J. (2020). The ERA5 Global Reanalysis. *Quarterly Journal of the Royal Meteorological Society*. doi: 10.1002/qj.3803

Holland, D. M., Thomas, R. H., Young, B. d., Ribergaard, M. H., & Lyberth, B. (2008). Acceleration of Jakobshavn Isbræ triggered by warm subsurface ocean waters. *Nature Geoscience*, *1*, 659. doi: 10.1038/ngeo316

Howat, I. M., Box, J., Ahn, Y., & Herrington, A. (2010). Seasonal variability in the dynamics of marine-terminating outlet glaciers in Greenland. *Journal of Glaciology*, *56*(198).

Howat, I. M., Joughin, I., Fahnestock, M., Smith, B., & Scambos, T. (2008). Synchronous retreat and acceleration of southeast Greenland outlet glaciers 2000–06: Ice dynamics and coupling to climate. *Journal of Glaciology*, *54*(187).

Howat, I. M., Joughin, I., & Scambos, T. A. (2007). Rapid Changes in Ice Discharge from Greenland Outlet Glaciers. *Science*, *315*(5818), 1559–1561. doi: 10.1126/science.1138478

Howat, I. M., Joughin, I., Tulaczyk, S., & Gogineni, S. (2005). Rapid retreat and acceleration of Helheim Glacier, east Greenland. *Geophysical Research Letters*, *32*(22), n/a–n/a. doi: 10.1029/2005GL024737

Inall, M., Murray, T., & Cottier, F. (2014). Oceanic heat delivery via Kangerdlugssuaq Fjord to the south-east Greenland ice sheet. *Journal of Geophysical Research: Oceans*, *119*(2). doi: 10.1002/2013jc009295

Jackson, R. H., & Straneo, F. (2016). Heat, Salt, and Freshwater Budgets for a Glacial Fjord in Greenland. *Journal of Physical Oceanography*, *46*(9), 2735–2768. doi: 10.1175/JPO-D-15-0134.1

Jackson, R. H., Straneo, F., & Sutherland, D. A. (2014). Externally forced fluctuations in ocean temperature at Greenland glaciers in non-summer months. *Nature Geoscience*, *7*(7), 503–508. doi: 10.1038/ngeo2186

Jaswal, A. K., Singh, V., & Bhambak, S. R. (2012). Relationship between sea surface temperature and surface air temperature over Arabian Sea, Bay of Bengal and Indian Ocean. *J. Ind. Geophys. Union*.

Jia, C. (2019). *Satellite Infrared Retrievals of Sea Surface Temperature at High* (Unpublished doctoral dissertation).

Johannessen, O. M., Korablev, A., Miles, V., Miles, M. W., & Solberg, K. E. (2011). Interaction Between the Warm Subsurface Atlantic Water in the Sermilik Fjord and Helheim Glacier in Southeast Greenland. *Surveys in Geophysics*, *32*(4-5), 387. doi: 10.1007/s10712-011-9130-6

Jones, C., Peterson, P., & Gautier, C. (1999). A New Method for Deriving Ocean Surface Specific Humidity and Air Temperature: An Artificial Neural Net-

work Approach. *Journal of Applied Meteorology*, *38*(8), 1229–1245. doi: 10.1175/1520-0450(1999)038⟨1229:anmfdo⟩2.0.co;2

Joughin, I., Alley, R. B., & Holland, D. M. (2012). Ice-Sheet Response to Oceanic Forcing. *Science*, *338*(6111), 1172–1176. doi: 10.1126/science.1226481

Kawai, Y., & Wada, A. (2007). Diurnal sea surface temperature variation and its impact on the atmosphere and ocean: A review. *Journal of Oceanography*, *63*(5), 721–744. doi: 10.1007/s10872-007-0063-0

Khan, S. A., Kjær, K. H., Bevis, M., Bamber, J. L., Wahr, J., Kjeldsen, K. K., ... Muresan, I. S. (2014). Sustained mass loss of the northeast Greenland ice sheet triggered by regional warming. *Nature Climate Change*, *4*(4), nclimate2161. doi: 10.1038/nclimate2161

Kilpatrick, K. A., Podestá, G., & Evans, R. (2001). Overview of the NOAA/NASA advanced very high resolution radiometer Pathfinder algorithm for sea surface temperature and associated matchup database. *Journal of Geophysical Research: Oceans*, *106*(C5), 9179–9197. doi: 10.1029/1999jc000065

Kilpatrick, K. A., Podestá, G., Walsh, S., Williams, E., Halliwell, V., Szczodrak, M., ... Evans, R. (2015). A decade of sea surface temperature from MODIS. *Remote Sensing of Environment*, *165*, 27–41. doi: 10.1016/j.rse.2015.04.023

Kilpatrick, K. A., Podestá, G., Williams, E., Walsh, S., & Minnett, P. J. (2019). Alternating Decision Trees for cloud masking in MODIS and VIIRS NASA sea-surface temperature products Alternating Decision Trees for cloud masking in MODIS and VIIRS NASA sea-surface temperature products. *Journal of Atmospheric and Oceanic Technology*. doi: 10.1175/JTECH-D-18-0103.1

King, M. D., Howat, I. M., Jeong, S., Noh, M. J., Wouters, B., Noël, B., & Broeke, M. R. v. d. (2018). Seasonal to decadal variability in ice discharge from the Greenland Ice Sheet. *The Cryosphere*, *12*(12), 3813–3825. doi: 10.5194/tc-12-3813-2018

Koizumi, M. (1956). Researches on the Variations of Oceanographic Conditions in the Region of the Ocean Weather Station “ Extra ” in the North Pacific Ocean (VI). *Papers in Meteorology and Geophysics*, *7*(3), 322–326. doi: 10.2467/mripapers1950.7.3_322

Konda, M., Imasato, N., & Shibata, A. (1996). A new method to determine near-sea surface air temperature by using satellite data. *Journal of Geophysical Re-*

search: Oceans, *101*(C6), 14349–14360. doi: 10.1029/96jc00796

Kraus, E. B., & Turner, J. S. (1967). A one-dimensional model of the seasonal thermocline II. The general theory and its consequences. *Tellus*, *19*(1), 98–106. doi: 10.1111/j.2153-3490.1967.tb01462.x

Kumar, A., Minnett, P. J., Podestá, G., & Evans, R. H. (2003). Error Characteristics of the Atmospheric Correction Algorithms Used in Retrieval of Sea Surface Temperatures from Infrared Satellite Measurements: Global and Regional Aspects. *Journal of the Atmospheric Sciences*, *60*(3), 575–585. doi: 10.1175/1520-0469(2003)060⟨0575:ecotac⟩2.0.co;2

Le Bras, I., Straneo, F., Holte, J., & Holliday, P. N. (2018). Seasonality of Freshwater in the East Greenland Current System From 2014 to 2016. *Journal of Geophysical Research: Oceans*. doi: 10.1029/2018JC014511

Luckman, A., Murray, T., Lange, R. d., & Hanna, E. (2006). Rapid and synchronous ice-dynamic changes in East Greenland. *Geophysical Research Letters*, *33*(3). doi: 10.1029/2005GL025428

McKinney, W. (2010). Data Structures for Statistical Computing in Python. , 56–61. doi: 10.25080/majora-92bf1922-00a

Millan, R., Rignot, E., Mouginot, J., Wood, M., Bjørk, A., & Morlighem, M. (2018). Vulnerability of Southeast Greenland Glaciers to Warm Atlantic Water From Operation IceBridge and Ocean Melting Greenland Data. *Geophysical Research Letters*, *45*(6), 2688–2696. doi: 10.1002/2017GL076561

Minnett, P. J. (2003). Radiometric measurements of the sea-surface skin temperature: the competing roles of the diurnal thermocline and the cool skin. *International Journal of Remote Sensing*, *24*(24), 5033–5047. doi: 10.1080/0143116031000095880

Minnett, P. J., Knuteson, R. O., Best, F. A., Osborne, B. J., Hanafin, J. A., & Brown, O. B. (2001). The Marine-Atmospheric Emitted Radiance Interferometer: A High-Accuracy, Seagoing Infrared Spectroradiometer. *Journal of Atmospheric and Oceanic Technology*, *18*(6), 994–1013. doi: 10.1175/1520-0426(2001)018⟨0994:tmaeri⟩2.0.co;2

Moon, T., Joughin, I., Smith, B., & Howat, I. (2012). 21st-Century Evolution of Greenland Outlet Glacier Velocities. *Science*, *336*(6081), 576–578. doi: 10.1126/science.1219985

Moore, G. W. K., Renfrew, I. A., Harden, B. E., & Mernild, S. H. (2015). The impact of resolution on the representation of southeast Greenland barrier winds and katabatic flows. *Geophysical Research Letters*, *42*(8), 3011–3018. doi: 10.1002/2015gl063550

Moore, G. W. K., Straneo, F., & Oltmanns, M. (2014). Trend and interannual variability in southeast Greenland Sea Ice: Impacts on coastal Greenland climate variability. *Geophysical Research Letters*, *41*(23), 8619–8626. doi: 10.1002/2014gl062107

Morlighem, M., Williams, C. N., Rignot, E., An, L., Arndt, J. E., Bamber, J. L., ... Zinglersen, K. B. (2017). BedMachine v3: Complete Bed Topography and Ocean Bathymetry Mapping of Greenland From Multibeam Echo Sounding Combined With Mass Conservation. *Geophysical research letters*, *44*(21), 11051–11061. doi: 10.1002/2017gl074954

Mouginot, J., Rignot, E., Scheuchl, B., Fenty, I., Khazendar, A., Morlighem, M., ... Paden, J. (2015). Fast retreat of Zachariæ Isstrøm, northeast Greenland. *Science*, *350*(6266), 1357–1361. doi: 10.1126/science.aac7111

Murray, T., Scharrer, K., James, T., Dye, S., Hanna, E., Booth, A., ... Huybrechts, P. (2010). Ocean regulation hypothesis for glacier dynamics in southeast Greenland and implications for ice sheet mass changes. *Journal of Geophysical Research: Earth Surface (2003–2012)*, *115*(F3). doi: 10.1029/2009JF001522

Ocean Biology Processing Group, O. E. L., NASA Goddard Space Flight Center. (2014a). *MODIS-Aqua Ocean Color Data.* https://earthdata.nasa.gov/. (Accessed: 2018-10-03) doi: http://dx.doi.org/10.5067/AQUA/MODIS_OC.2014.0

Ocean Biology Processing Group, O. E. L., NASA Goddard Space Flight Center. (2014b). *MODIS-Terra Ocean Color Data.* https://earthdata.nasa.gov/. (Accessed: 2018-10-03) doi: http://dx.doi.org/10.5067/TERRA/MODIS_OC.2014.0

Oltmanns, M., Straneo, F., Moore, G., & Mernild, S. (2014). Strong Downslope Wind Events in Ammassalik, Southeast Greenland. *Journal of Climate*, *27*(3), 977–993. doi: 10.1175/JCLI-D-13-00067.1

Price, J. F., Weller, R. A., & Pinkel, R. (1986). Diurnal cycling: Observations and models of the upper ocean response to diurnal heating, cooling,

and wind mixing. *Journal of Geophysical Research*, *91*(C7), 8411. doi: 10.1029/jc091ic07p08411

Rignot, E., & Kanagaratnam, P. (2006). Changes in the velocity structure of the Greenland Ice Sheet. *Science*, *311*.

Rudels, B., Fahrbach, E., Meincke, J., Budéus, G., & Eriksson, P. (2002). The East Greenland Current and its contribution to the Denmark Strait overflow. *ICES Journal of Marine Science*, *59*(6), 1133–1154. doi: 10.1006/jmsc.2002.1284

Schild, K. M., & Hamilton, G. S. (2013). Seasonal variations of outlet glacier terminus position in Greenland. *Journal of Glaciology*, *59*(216), 759–770. doi: 10.3189/2013jog12j238

Schulz, J., Meywerk, J., Ewald, S., & Schlüssel, P. (1997). Evaluation of Satellite-Derived Latent Heat Fluxes. *Journal of Climate*, *10*(11), 2782–2795. doi: 10.1175/1520-0442(1997)010⟨2782:eosdlh⟩2.0.co;2

Seabold, S., & Perktold, J. (2010). Statsmodels: Econometric and Statistical Modeling with Python. , 92–96. doi: 10.25080/majora-92bf1922-011

Shepherd, A., Ivins, E. R., Geruo, A., Barletta, V. R., Bentley, M. J., Bettadpur, S., ... Zwally, J. H. (2012). A Reconciled Estimate of Ice-Sheet Mass Balance. *Science*, *338*(6111), 1183–1189. doi: 10.1126/science.1228102

Singh, R., Joshi, P. C., & Kishtawal, C. M. (2006). A new method to determine near surface air temperaturefrom satellite observations. *International Journal of Remote Sensing*, *27*(14), 2831–2846. doi: 10.1080/01431160500195234

Singh, R., Kishtawal, C. M., & Joshi, P. C. (2005). Estimation of monthly mean air-sea temperature difference from satellite observations using genetic algorithm. *Geophysical Research Letters*, *32*(2). doi: 10.1029/2004gl021531

Spreen, G., Kaleschke, L., & Heygster, G. (2008). Sea ice remote sensing using AMSR-E 89-GHz channels. *Journal of Geophysical Research*, *113*(C2). doi: 10.1029/2005jc003384

Stearns, L. A., & Hamilton, G. S. (2007). Rapid volume loss from two East Greenland outlet glaciers quantified using repeat stereo satellite imagery. *Geophysical Research Letters*, *34*(5). doi: 10.1029/2006gl028982

Stramma, L., Cornillon, P., Weller, R. A., Price, J. F., & Briscoe, M. G. (1986). Large Diurnal Sea Surface Temperature Variability: Satellite and In Situ Measurements. *Journal of Physical Oceanography*, *16*(5), 827–837. doi:

10.1175/1520-0485(1986)016⟨0827:ldsstv⟩2.0.co;2

Straneo, F., Curry, R., Sutherland, D., & Hamilton, G. (2011). Impact of fjord dynamics and glacial runoff on the circulation near Helheim Glacier. *Nature Geoscience*, *4*. doi: 10.1038/ngeo1109

Straneo, F., Hamilton, G., Stearns, L., & Sutherland, D. (2016). Connecting the Greenland Ice Sheet and the Ocean: A Case Study of Helheim Glacier and Sermilik Fjord. *Oceanography*, *29*(4), 34–45. doi: 10.5670/oceanog.2016.97

Straneo, F., Hamilton, G. S., Sutherland, D. A., Stearns, L. A., Davidson, F., Hammill, M. O., ... Rosing-Asvid, A. (2010). Rapid circulation of warm subtropical waters in a major glacial fjord in East Greenland. *Nature Geoscience*, *3*(3), 182. doi: 10.1038/ngeo764

Straneo, F., & Heimbach, P. (2013). North Atlantic warming and the retreat of Greenland's outlet glaciers. *Nature*, *504*(7478), 36–43. doi: 10.1038/nature12854

Straneo, F., Sutherland, D. A., Holland, D., Gladish, C., Hamilton, G. S., Johnson, H. L., ... Koppes, M. (2012). Characteristics of ocean waters reaching Greenland's glaciers. *Annals of Glaciology*, *53*(60), 202–210. doi: 10.3189/2012aog60a059

Stroh, J. N., Panteleev, G., Kirillov, S., Makhotin, M., & Shakhova, N. (2015). Sea-surface temperature and salinity product comparison against external in situ data in the A rctic O cean. *Journal of Geophysical Research: Oceans*, *120*(11), 7223–7236. doi: 10.1002/2015jc011005

Sutherland, D. A., & Pickart, R. S. (2008). The East Greenland Coastal Current: Structure, variability, and forcing. *Progress in Oceanography*, *78*(1), 58–77. doi: 10.1016/j.pocean.2007.09.006

Sutherland, D. A., Pickart, R. S., Jones, P. E., Azetsu-Scott, K., Eert, J. A., & Ólafsson, J. (2009). Freshwater composition of the waters off southeast Greenland and their link to the Arctic Ocean. *Journal of Geophysical Research*, *114*(C5). doi: 10.1029/2008JC004808

Sutherland, D. A., Straneo, F., & Pickart, R. S. (2014). Characteristics and dynamics of two major Greenland glacial fjords. *Journal of Geophysical Research: Oceans*, *119*(6), 3767–3791. doi: 10.1002/2013JC009786

Sutherland, D. A., Straneo, F., Stenson, G. B., Davidson, F., Hammill, M. O., & Rosing-Asvid, A. (2013). Atlantic water variability on the SE Greenland continental shelf and its relationship to SST and bathymetry. *Journal of Geophysical Research: Oceans*, *118*(2), 847–855. doi: 10.1029/2012JC008354

Sverdrup, H. U., Johnson, M. W., & Fleming, R. H. (1942). *The Oceans: Their Physics, Chemistry, and General Biology*. New York: Prentice-Hall, Inc. Retrieved from `http://ark.cdlib.org/ark:/13030/kt167nb66r/`

Szczodrak, M., Minnett, P. J., & Evans, R. H. (2014). The effects of anomalous atmospheres on the accuracy of infrared sea-surface temperature retrievals: Dry air layer intrusions over the tropical ocean. *Remote Sensing of Environment*, *140*, 450–465. doi: 10.1016/j.rse.2013.09.010

The IMBIE Team. (2019). Mass balance of the Greenland Ice Sheet from 1992 to 2018. *Nature*. doi: 10.1038/s41586-019-1855-2

van den Broeke, M., Bamber, J., Ettema, J., Rignot, E., Schrama, E., Berg, W. v. d., ... Wouters, B. (2009). Partitioning Recent Greenland Mass Loss. *Science*, *326*(5955), 984–986. doi: 10.1126/science.1178176

Virtanen, P., Gommers, R., Oliphant, T. E., Haberland, M., Reddy, T., Cournapeau, D., ... Vázquez-Baeza, Y. (2019). SciPy 1.0–Fundamental Algorithms for Scientific Computing in Python. *arXiv*, *17*(3), 261–272. doi: 10.1038/s41592-019-0686-2

Våge, K., Pickart, R. S., Sarafanov, A., Knutsen, , Mercier, H., Lherminier, P., ... Bacon, S. (2011). The Irminger Gyre: Circulation, convection, and interannual variability. *Deep Sea Research Part I: Oceanographic Research Papers*, *58*(5), 590–614. doi: 10.1016/j.dsr.2011.03.001

Walsh, K. M., Howat, I. M., Ahn, Y., & Enderlin, E. M. (2012). Changes in the marine-terminating glaciers of central east Greenland, 2000–2010. *The Cryosphere*, *6*(1), 211–220. doi: 10.5194/tc-6-211-2012